RMetS
Royal Meteorological Society

Ocean ensemble forecasting. Part II: Mediterranean Forecast System response

Nadia Pinardi,[a] Alessandro Bonazzi,[b] Srdjan Dobricic,[c] Ralph F. Milliff,[d]* Christopher K. Wikle[e] and L. Mark Berliner[f]

[a]*CIRSA, University of Bologna, Ravenna, Italy*
[b]*Operational Oceanography Group, INGV, Bologna, Italy*
[c]*Centro EuroMediterraneo per i Cambiamenti Climatici, Bologna, Italy*
[d]*NWRA, Colorado Research Associates Div., Boulder, CO, USA*
[e]*Statistics Department, University of Missouri, Columbia, MO, USA*
[f]*Statistics Department, Ohio State University, Columbus, OH, USA*
*Correspondence to: R. F. Milliff, NorthWest Research Associates, Colorado Research Associates Division, 3380 Mitchell Lane, Boulder, Colorado 80301, USA. E-mail: milliff@cora.nwra.com

This article analyzes the ocean forecast response to surface vector wind (SVW) distributions generated by a Bayesian hierarchical model (BHM) developed in Part I of this series. A new method for ocean ensemble forecasting (OEF), the so-called BHM-SVW-OEF, is described. BHM-SVW realizations are used to produce and force perturbations in the ocean state during 14 day analysis and 10 day forecast cycles of the Mediterranean Forecast System (MFS). The BHM-SVW-OEF ocean response spread is amplified at the mesoscales and in the pycnocline of the eddy field. The new method is compared with an ensemble response forced by European Centre for Medium-Range Weather Forecasts (ECMWF) ensemble prediction system (EEPS) surface winds, and with an ensemble forecast started from perturbed initial conditions derived from an ad hoc thermocline intensified random perturbation (TIRP) method. The EEPS-OEF shows spread on basin scales while the TIRP-OEF response is mesoscale-intensified as in the BHM-SVW-OEF response. TIRP-OEF perturbations fill more of the MFS domain, while the BHM-SVW-OEF perturbations are more location-specific, concentrating ensemble spread at the sites where the ocean-model response to uncertainty in the surface wind forcing is largest.

Key Words: forecast uncertainty; wind perturbations; model error structure; mesoscales; upper ocean variability; Bayesian hierarchical methods

Received 13 November 2009; Revised 16 February 2011; Accepted 28 February 2011; Published online in Wiley Online Library 3 May 2011

Citation: Pinardi N, Bonazzi A, Dobricic S, Milliff RF, Wikle CK, Berliner LM. 2011. Ocean ensemble forecasting. Part II: Mediterranean Forecast System response. *Q. J. R. Meteorol. Soc.* **137**: 879–893. DOI:10.1002/qj.816

1. Introduction

The aims of this article are (1) to analyze the impact of the Bayesian hierarchical model (BHM) surface vector winds (SVW), hereafter BHM-SVW, derived in Part I of this series (Milliff *et al.*, 2011) on the ocean ensemble forecast (OEF) response and (2) to compare the response with other ensemble-forecast-generating methods. The assessment will be carried out for the short-term, open-ocean Mediterranean Forecasting System (MFS: Pinardi *et al.*, 2003; Pinardi and Coppini, 2010). The MFS produces deterministic ten-day ocean forecasts starting from ocean analyses that incorporate

both satellite and *in situ* data. The MFS ocean forecasting model is eddy-resolving and mesoscale variability dominates the flow field on weekly time-scales. Phase and amplitude errors associated with the growth, decay and propagation of the eddies are the main causes of forecast predictability loss. Forecast errors in temperature, salinity and sea level double on time-scales of a few days (Tonani *et al.*, 2009).

Given that the predictability limit of short-term ocean forecasting is associated with oceanic mesoscale eddies, any ocean ensemble forecasting method should consider both initial conditions and atmospheric forcing errors. The impacts of high-resolution and high-intensity scatterometer winds on the ocean response have been documented in prior work (Milliff *et al.*, 1999, 2001), showing that high-resolution winds affect both the mesoscale and the time-mean circulation. In particular, the high-resolution properties of scatterometer winds are necessary to force deep mixing events, ocean upwelling and ocean-eddy variability (Kersalé *et al.*, 2010) accurately. Thus, we hypothesize that inputs from scatterometer winds are essential in the development of a probabilistic ensemble ocean forecast system, focused on ocean mesoscales. Starting from the uncertainty in atmospheric SVW fields, Part I of this article constructed an ensemble of initial conditions consistent with the assimilation of ocean observations and atmospheric wind errors during the analysis cycle of the MFS. This article will now study the characteristics of the ten-day OEF standard deviation, i.e. the spread, derived from ensemble initial conditions and BHM-SVW forecast wind realizations.

The BHM-SVW-OEF spread will be compared with the ensemble standard deviation produced with (1) wind realizations coming from the European Centre for Medium-Range Weather Forecasts (ECMWF) Ensemble Prediction System (EEPS) and (2) a fixed initial-condition perturbation method, already shown to be efficient for producing spread on ocean mesoscales (Pinardi *et al.*, 2008). The EEPS forcing members display large-scale differences (Buizza, 2006), while the differences in BHM-SVW realizations are broad-band and include high wave-number signals. These differences are explored in greater detail in section 3.3 of this article. The sensitivity of the OEF spread to the ocean forecast model horizontal resolution will also be studied for both the BHM-SVW and ECMWF EPS ensemble-generating methods.

The impact of wind forcing errors on ocean ensemble forecasts has been studied by other authors. Andreu-Burillo *et al.* (2002) developed a pseudo-random perturbation method for winds and performed 100 forecasts with the same initial condition, generating an ensemble spread in the mixed layer (first 100 m). Auclair *et al.* (2003) again used pseudo-random perturbations of the winds, initial density, lateral boundary conditions and river inputs, for a coastal model domain. They showed that the model response spread is sensitive to each perturbation type depending on the dominant ocean-current regime. Lucas *et al.* (2008) perturbed winds, air temperature and incoming solar radiation fields, deducing the errors from the comparison of the ECWMF re-analysis forcing fields with data from the Co-ordinated Ocean-Ice Reference Experiments (CORE). Again, the perturbations to the ECMWF re-analysis fields were modelled in a pseudo-random way and the ocean response peaked in the eddy field of the Gulf Stream and tropical regions of the North Atlantic. However, the perturbations at 100 m needed several months to grow, limiting the utility for real-time daily ensemble forecasting systems. These previous attempts did not use realistic estimates of the atmospheric wind errors such as we have developed with the BHM-SVW method and they did not use model-adjusted initial-condition perturbations, as we have shown in Part I of this article (Milliff *et al.*, 2011).

In section 2 we describe the main characteristics of the MFS operational ocean forecasting system and the different resolution models used in this article. Section 3 describes the two ensemble-generating methods from BHM-SVW and EEPS winds and section 4 offers the comparison of ensemble responses with the two methods. Section 5 describes an alternative initial-condition perturbation method and a comparison with the previous ensemble results. Section 6 describes the vertical temperature and salinity structure of the ensemble variance generated by the BHM-SVW-OEF method and section 7 provides a summary and conclusions.

2. The Mediterranean Forecasting System: assimilation scheme and models

The MFS* is composed of a large observational network, a numerical prediction model and a data-assimilation scheme. The observational network consists of real-time satellite and *in situ* data. The latter include temperature vertical profiles down to 700 m provided by a 'ship of opportunity' programme (Manzella *et al.*, 2007) and temperature and salinity profiles down to 700 and 2000 m implemented by the MedArgo program (Poulain *et al.*, 2007). The real-time satellite measurements include along-track sea-level anomaly (SLA) from altimetry (Le Traon *et al.*, 2003) and sea-surface temperature (SST: Buongiorno-Nardelli *et al.*, 2003).

The MFS ocean model is described in Tonani *et al.* (2008) and here we outline only its main characteristics. The model has 71 non-uniform z-coordinate levels and a horizontal resolution of $1/16^\circ \times 1/16^\circ$. The model domain covers the Mediterranean Sea and a portion of the Atlantic Ocean where an Atlantic box is designed to parametrize coupling between the Mediterranean and the Atlantic. The operational model is forced by ECMWF surface fields using interactive air–sea physics (Pinardi *et al.*, 2003). A lower resolution implementation of the MFS numerical ocean model, with 71 vertical levels and a horizontal resolution of $1/4^\circ \times 1/4^\circ$, is also used in this article. The geographical domain of the low-resolution model is the same as that of the high-resolution model except for the Atlantic box, which is taken from previous investigations at the lower resolution (Korres *et al.*, 2000; Brankart and Pinardi, 2001). In the following, the high- and low-resolution versions of the MFS models are referred to as MFS1671 and MFS471 respectively. The MFS471 model is initialized from MFS1671 fields using bilinear interpolation.

The atmospheric forcing used in the MFS is derived from the ECMWF analysis fields and the ten-day ECMWF single deterministic forecast fields, starting at 1200 UTC. Deterministic forecast winds are generated twice a day by the ECMWF atmospheric model starting from an analyzed initial condition and integrating forward in time for the next ten days. In addition to this deterministic system, the ECMWF operational model once a day runs a 51 member ensemble prediction system that will be described in

*http://gnoo.bo.ingv.it/mfs

section 3.2. The ECMWF forecast model has a spectral representation with a triangular truncation of 511 waves in the horizontal and 60 levels in the vertical ($T511L60$), which means a nominal horizontal resolution of 40 km. The surface fields are utilized in a reduced regular grid of 0.5×0.5 degrees of latitude and longitude. The ECMWF surface winds, mean sea-level pressure, air temperature, relative humidity and cloud cover are used in bulk formulae (Pettenuzzo *et al.*, 2010) that, combined with the model SST, provide momentum and heat fluxes to the ocean model. The ocean operational outputs that use the deterministic ECMWF SVW analysis and forecast fields will hereafter be called the control.

All the real-time data are assimilated in both ocean models using a reduced-order optimal interpolation scheme adapted by Dobricic *et al.* (2007) to produce daily ocean analyses. Ocean state analyses are constructed using ECMWF surface-analysis forcing fields and by assimilating available ocean data using a one-day temporal window. The error-covariance matrix is a reduced-order, multivariate matrix, described in detail in Dobricic *et al.* (2005). The order reduction results from the decomposition of the error covariance into leading vertical and horizontal modes. The vertical modes are multivariate temperature, salinity and sea-surface height (SSH) empirical orthogonal functions (EOFs) for different regions and seasons in the Mediterranean Sea. The assimilation scheme is sequential and at the end of each day the error-covariance matrix is used to correct the background model fields, producing an analysis snapshot, considered as initial condition for the next day's analysis or forecast.

In Figure 1, the MFS analysis and control forecast cycle are schematized. At day J of the week, a 14 day analysis period is started from day $J - 14$ to $J - 1$, producing $1A$–$14A$ analysis fields. A control forecast is then started from the $14A$ analysis snapshot (Day 0 of the forecast period), producing $1F$–$10F$ control forecast fields. Both MFS1671 and MFS471 models use the same assimilation scheme, observational data and deterministic atmospheric forcings.

3. Ocean ensemble methods generated by wind ensembles

In the following two subsections we will describe the two ocean ensemble forecast methods that use wind-forcing perturbations to generate ocean ensemble forecasts.

3.1. The BHM-SVW ocean ensemble forecast method

The BHM-SVW posterior distributions, developed in Part I of this article (Milliff *et al.*, 2011) are used to design a new ensemble forecast method, the so-called BHM-SVW ocean ensemble forecast (OEF) method. As detailed in Part I, the BHM-SVW is a probabilistic model, the output of which is the posterior distribution of the SVW at each grid location for each output time (i.e. every 6 h on a regular 0.5° grid). According to Bayes' theorem, the posterior distribution results from the normalized product of a data-stage distribution and a process-model distribution (multiplied by marginal distributions for the parameters arising in data and process models; see Part I). Parameters of the data-stage distribution account for observational errors (i.e. from scatterometer winds) and analysis and forecast errors (i.e. from ECMWF fields). Parameters of the process-model distribution represent terms and uncertainties in the stochastic equation representation of the Rayleigh friction equations (see Part I). The high-resolution, high-accuracy data-stage inputs from scatterometer winds provide the SVW posterior distributions with realistic kinetic energies at high wave numbers. The high wave-number properties of the BHM-SVW realizations drive localized spread in the initial condition members at $14A$, as shown in Part I, section 5.2. The error-covariance matrix is identical for each BHM-SVW-EOF member during the analysis period and thus the $14A$ initial conditions differ only because of the BHM-SVW realizations used to force the model.

The differences with respect to other existing methods are twofold: (1) the wind realizations force the models during the assimilation cycle in order to produce initial-condition perturbations and (2) the BHM-SVW realizations transition smoothly between the analysis and forecast periods. The first feature ensures that perturbations grow in the ocean field only where observations are not sufficient to reduce the initial-condition uncertainty. The second feature ensures that the ensemble forecast and analysis wind fields have distribution variances that are smoothly changing across the analysis and forecast periods.

The BHM-SVW-OEF method is then designed as follows (Figure 1). During the 14 day analysis period, each ocean ensemble member is forced with a different BHM-SVW realization, while assimilating the ocean temperature, salinity and SLA observations. The n ocean initial conditions produced at day J are then forced with the corresponding n BHM-SVW realizations in the forecast period: n is 10 for MFS1671 and 100 for MFS471. The cost of integrating MFS1671 constrains the ensemble size even though the greater number of degrees of freedom in the higher-resolution model might justify a larger n. It is important to note that the BHM-SVW realizations produce not only perturbed wind stresses and thus momentum fluxes, but also perturbed surface heat and water fluxes as well. Using interactive bulk formulae in the model together with BHM-SVW perturbs all surface fluxes affected by uncertainty in surface winds.

3.2. The EEPS ocean ensemble forecast method

The second ocean ensemble forecast method studied in this article uses SVW realizations from the ECMWF ensemble prediction system (EEPS). We call this method the EEPS ocean ensemble forecast (EEPS-OEF). EEPS for the global atmosphere has proven to be useful in a wide range of applications (Buizza, 2006). However, the utility of EEPS surface winds as forcing to generate ocean ensemble forecasts has not been tested. It will be compared here with the BHM-SVW-OEF method.

EEPS uses singular vectors to perturb the atmospheric forecast initial conditions (Lacarra and Talagrand, 1988; Farrell, 1990). The singular vectors identify patterns with maximum growth rates within the first 48 h of the forecast and for synoptic scales. Small errors in the initial-condition state will amplify most rapidly in patterns corresponding to the leading singular vectors, and will affect the forecast accuracy (Buizza and Palmer, 1995). Since the end of 2000 and up to 2005, the operational implementation of the EEPS includes 50 perturbed members at $T255L62$ resolution, plus an unperturbed forecast (i.e. 51 ensemble members in total). The nominal resolution of the EEPS winds is approximately

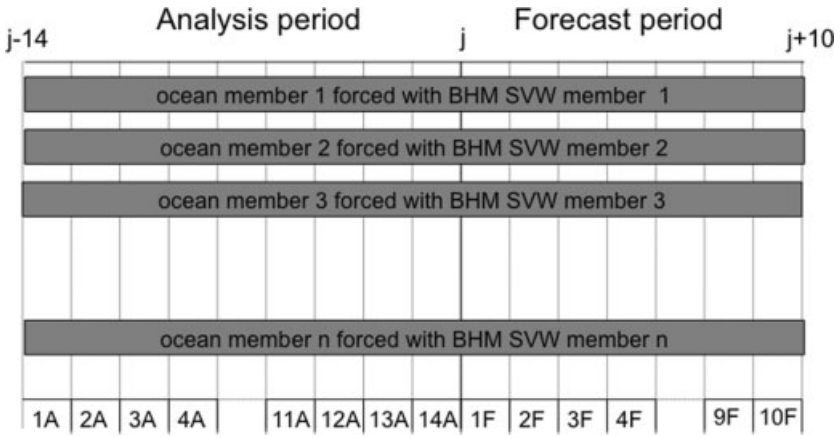

Figure 1. Schematic of the MFS analysis and forecast control cycle and the BHM-SVW-OEF method: *J* indicates the day at which the forecasts start, 1*A*–14*A* and 1*F*–10*F* indicate analysis and forecast days respectively. The *n* BHM-SVW realizations are used to force OEF members starting from different analysis initial conditions created at 14*A*.

80 km, i.e. two times lower than the deterministic ECMWF forecast winds.

The EEPS-OEF method makes use of a single analysis field snapshot at 14*A* as the initial condition for the ocean forecast. For the high-resolution model, MFS1671, 10 forecasts are forced by EEPS wind members. For the low-resolution model, MFS471, all 51 members of the EEPS are used. The EEPS-OEF method has a clear disadvantage in terms of producing useful spread in the ensemble forecast, since it starts from an unperturbed initial condition.

3.3. *Comparison between BHM and EEPS SVW distributions*

Figure 2 shows the posterior SVW amplitude standard deviation generated by the BHM and EEPS, and a comparison with the root-mean-square (rms) forecast error. The latter is defined as the rms of the difference between ECMWF 10 day deterministic wind forecasts and the corresponding wind analyses, computed for 255 10 day forecast periods in the years 2000–2004 and averaged over the basin. The BHM-SVW and the EEPS wind spread are instead calculated for the period from 25 January–17 February 2005 only. For EEPS the spread is calculated as the standard deviation from the mean of the 51 ensemble members. The BHM-SVW amplitude, $W(x, y, t) = |\mathbf{U}|$, is calculated from the BHM-SVW realizations and the distribution is given by

$$W(x, y, t) \sim N[W_{\text{mean}}(x, y, t), \sigma_W^2]; \qquad (1)$$

for notation see Part I (Milliff *et al.*, 2011), where x, y, t denote space and time coordinates and σ_W is the standard deviation represented in Figure 2, which provides a succinct depiction of the important differences in probabilistic BHM-SVW (red) and deterministic EEPS wind (blue) forcing-ensemble standard deviations. The variances in the wind forcing ensembles over the forecast time provide a context for the comparison of ocean ensemble forecast results.

Clearly, different concepts of uncertainty are being implemented in the EEPS and BHM-SVW distributions. For the BHM-SVW case, the uncertainties in the surface wind during the analysis period derive from parameters selected to represent observational errors (i.e. for QuikSCAT and ECMWF analysis winds) and process-model errors.

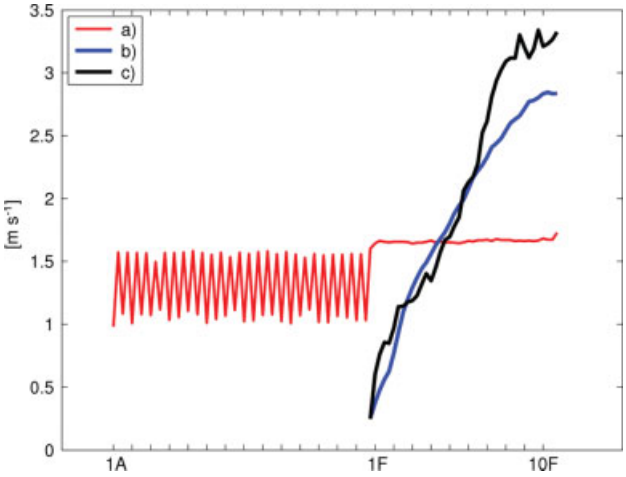

Figure 2. Comparison of wind amplitude spread for different wind ensemble-generating methods and the ECMWF surface wind forecast errors. (a) Wind amplitude spread σ_W (see Eq. (1)) of the BHM-SVW distribution during analysis and forecast periods (25 January–7 February 2005 (1*A*–14*A*), 8–17 February 2005 (1*F*–10*F*)). b) As (a) but for EEPS winds during the forecast period. (c) ECMWF rms forecast error computed for the period 2000–2004 and averaged over the basin.

During the forecast period, the error parameters represent uncertainties in the ECMWF forecast winds and the process model. Figure 2 shows that the spread varies periodically during the period 1*A*–14*A* due to the insertion of scatterometer data. The spread remains constant during the forecast period, since the ECMWF forecast wind variance has been modelled as time-independent (see Milliff *et al.*, 2011). The EEPS wind spread (blue curve) instead mimics the growth of the forecast error (black curve), albeit offset to lower amplitude after day 6*F*. The BHM-SVW amplitude spread during the 1*F*–10*F* period is slightly larger than 1.5 m s^{-1}, which is the spread of EEPS winds and the forecast error at day 5*F*.

It is important to note the difference between EEPS and BHM SVW distribution spreads at 1*F*. The BHM-SVW method smoothly carries the variance information from the analysis time to the forecast period without discontinuities. EEPS instead grows from almost zero at the forecast initial time to a value larger than 2.5 m s^{-1}. This rapid error growth may cause unwanted response in the ocean forecast ensemble

and contamination by ocean surface gravity waves, as has been shown in other articles (Powell *et al.*, 2009).

In order better to describe the differences between EEPS and BHM-SVW distributions, Figure 3 shows snapshots of the SVW and wind curl from the two data sets in the northwestern Mediterranean Sea during a Mistral event occurring on 14 February 2005, i.e. day 7*F*. Three realizations are shown from the EEPS and BHM-SVW ensemble winds. The amplitude of the wind curl is larger in the deterministic forecast winds (indicated as 'control') compared with the EEPS, probably due to the low resolution of the EPS atmospheric model as described before. EEPS members differ in synoptic-scale patterns while the BHM-SVW are different at finer spatial scales, i.e. subsynoptic or atmospheric mesoscales. The scales of uncertainty given by these two wind ensembles are not overlapping, since the EEPS distributions focus on the error growth in the 500 hPa geopotential height field while the BHM-SVW distributions focus on the surface wind errors as characterized by QuikSCAT. Our analyses indicate that the surface atmospheric flow field exhibits finer spatial scale errors, probably due to orographic effects and land–sea temperature and humidity differences. In the sections below, we will show that the smaller-scale uncertainties in the wind-field realizations are important in generating an ensemble response at the ocean mesoscale.

4. Comparison of BHM-SVW and EEPS ocean ensemble forecast methods

In this section we compare the ocean responses of the two ensemble ocean forecast perturbation methods described in the previous section for the high-resolution MFS1671 and low-resolution MFS471 model systems. The ocean ensemble forecast initial conditions are generated by BHM-SVW-OEF during the period 25 January–7 February 2005 (1*A*–14*A*), while the forecast period is from 8–17 February 2005 (1*F*–10*F*). This ensemble forecast case study is carried out in parallel with the control MFS forecast for the same period.

The ocean initial-condition spread for the BHM-SVW-OEF with MFS1671 has been discussed in Part I (Milliff *et al.*, 2011). We have shown there that the initial-condition spread in SSH and SST is located in specific regions of the basin, where we suspect that ocean hydrodynamic instabilities, eddy interaction and eddy propagation processes are occurring.

4.1. *High-resolution model ensemble response*

Figure 4 compares the BHM-SVW-OEF and EEPS-OEF responses at the end of the forecast period (day 10*F*, 17 February 2005) for the MFS1671 model. The daily mean SSH for the control forecast at day 10*F* (Figure 4(a)) shows high SSH and intense gradients along the southern coastlines of the basin and along the northern Levantine coastline, off Turkey. Local maxima occur in the Algerian current (6°E, 38.5°N) and in the area of the Mersa-Matruh gyre (29°E, 32°N). Sub-basin-scale cyclonic gyre circulations are indicated by SSH minima in the Gulf of Lyon (5°E, 42°N), the central Ionian Sea (19°E, 38°N) and the Rhodes Gyre region of the Levantine Sea (27.5°E, 35°N).

Figure 4(b) shows that the BHM-SVW-OEF spread is localized in specific regions, at the scale of the eddies, and it has doubled in amplitude from the initial-condition values (see figure 9 of Part I: Milliff *et al.*, 2011). The spread is associated with large gradients in the SSH field that identify currents (i.e. the Algerian current in the western basin from 0–10°E, the Atlantic–Ionian Stream in the central Ionian Sea from 15–20°E and the North African current up to the western edge of the Mersa Matruh Gyre in the Levantine basin from 20–30°E). In these regions, the SSH spread for BHM-SVW-OEF reaches values of 6 cm. On the other hand, spread for the EEPS-OEF method (Figure 4(c)) is large everywhere and non-localized (i.e. a basin-wide uniform value of approximately 2.5 cm). Additional amplitude in SSH spread for the EEPS-OEF occurs in the Aegean Sea, the Adriatic Sea and the Gulf of Gabes (10°E, 34°N), as well as in the same regions identified for BHM-SVW-OEF but at smaller amplitude. On the other hand, low spread is evident in the Sicily Strait and the near-shore areas of the Algerian current, where dominant winds probably have low variance.

For both methods, the average response spread is relatively small (order 3 cm) and comparable to the SLA satellite errors (Dobricic *et al.*, 2005). The area of maximum ocean response spread corresponds to the large-variance areas in the BHM-SVW realizations, as shown for example in figure 7 of Part I. However, not all the areas of high BHM-SVW spread generate an ocean response spread and this is probably due to the presence of unstable ocean dynamical features that can amplify the perturbations given by the BHM-SVW winds. The Algerian current seems to be a region that amplifies the ocean response to the wind uncertainty during the assimilation and the forecast periods we have analyzed (see Part I and Part II of this article respectively).

The highest ensemble variance values are observed in both the BHM-SVW-OEF and EEPS-OEF responses at the location of the Algerian current anticyclonic eddies, one of which during this period is centred at 6°E, 38.5°N. Figure 5 shows how this structure is represented in the ensemble responses to both the BHM-SVW-OEF and EEPS-OEF. Figure 5 also depicts the effect of evolving currents in three ensemble members for each method on the simulated trajectories of six drifters released at the centre of the anticyclone in each member at day 1*F* and tracked through day 10*F*. In this depiction, it is clear that the BHM-SVW-OEF members present a wider range of possible states than the EEPS-OEF members. A mesoscale eddy structure has detached in the period between 1*F* and 10*F* (not shown) from the northeastern edge of the anticyclone in BHM-SVW-OEF members 1 and 2, but not in member 3. The western border of the anticyclone is interacting with a second smaller eddy in BHM-SVW-OEF members 1 and 3, but this process is almost absent in BHM-SVW-OEF member 2. The cyclonic circulation north of the anticyclone strengthens in member 2 and not in the others. Conversely, the three EEPS-OEF members do exhibit similar variability, being different only in the strengthening/weakening of the cyclonic synoptic eddy on the northern border of the anticyclone. The simple trajectory simulations allow us better to visualize the effect of the uncertainty on the dynamical evolution of the anticyclonic eddy due to the deterministic components of the particle trajectories, since no random dispersion due to Lagrangian subgrid scales was considered. In this simplified framework, we observe that the EEPS-OEF does not allow for any of the particles to exit the anticyclonic eddy, while the BHM-SVW-OEF exhibits a greater spread, i.e. members 2 and 3 show several

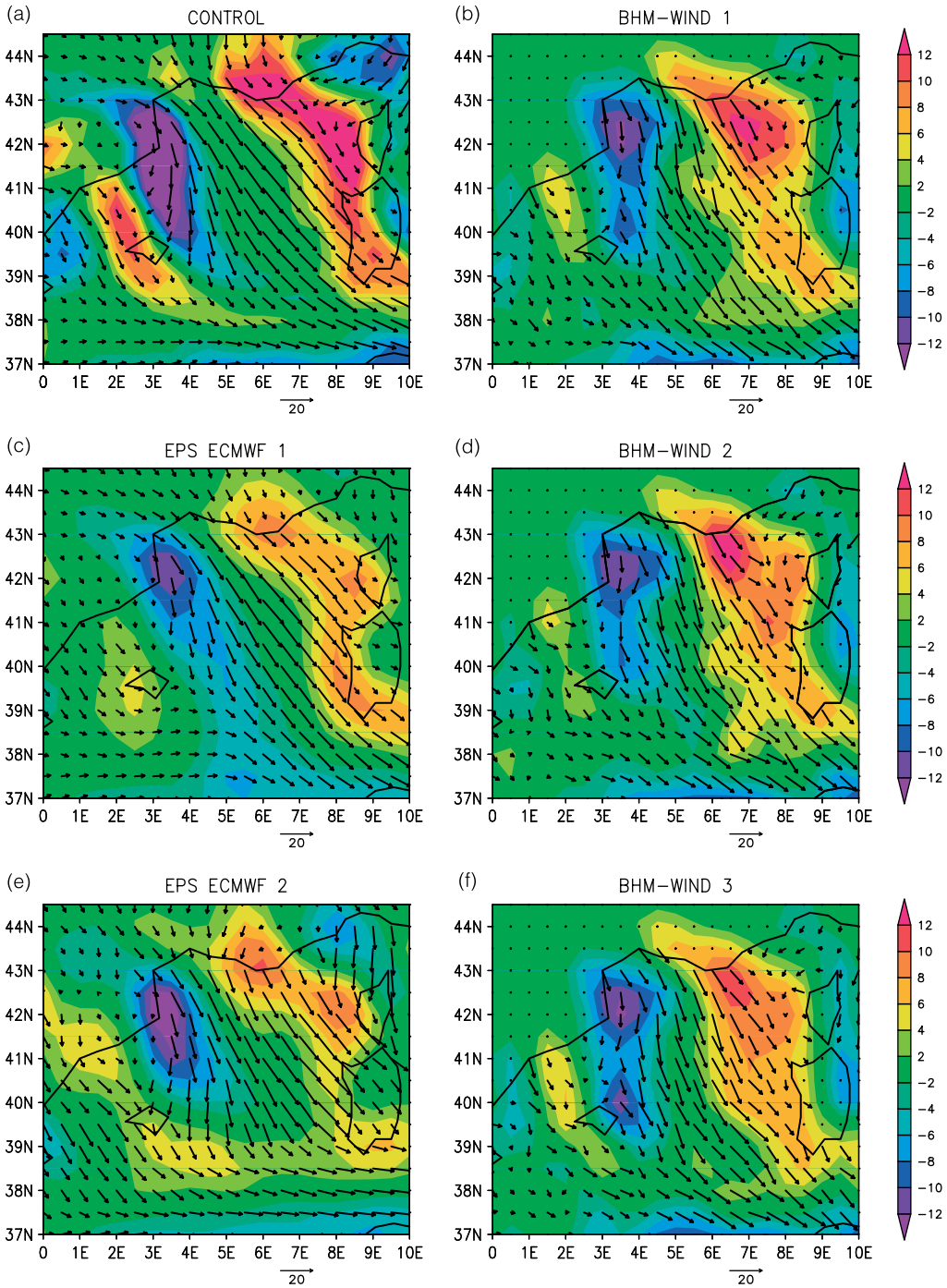

Figure 3. Western Mediterranean wind fields from three realizations of the EEPS (left column, including the unperturbed EPS fields at the top left) and the BHM-SVW (right column). Surface winds (vectors, m s^{-1}) and wind curl (colour contours, N $m^{-3} * 10^6$) for 14 February 2005 at 0000 UTC, day 7*F*.

particles escaping the eddy centre in different directions. Figures 3 and 5 are consistent in that the EEPS winds do not contain spatial variability at length-scales commensurate with the ocean mesoscale, while the BHM-SVW realizations do. This variability at high wave numbers in BHM-SVW (also demonstrated in the spectra from Part I) drives greater ensemble spread in the SSH response over the course of the ocean forecast. Figure 5 demonstrates this in two ways. Firstly, the SSH contours (colour) for each realization exhibit widely different morphologies for each BHM-SVW realization (right column) versus the very similar morphologies even at day 10*F* in the realizations forced by EEPS (left column). Secondly, the particle trajectories tracked over all 10 forecast days for each realization suggest that the spread differences are evident throughout the 10 days of the forecast.

Isern-Fontanet *et al.* (2006) explained the dynamics of similar Algerian current anticyclonic eddies in terms of two-dimensional turbulence. In particular, they showed that the high current amplitude rim of the eddy is characterized by shear stresses and strains that can cause large changes in the paths of drifters released in the eddy core. Our results show that forcing with realizations from a SVW posterior distribution that is consistent with uncertainties in the wind observations produces differences in the eddy rim circulation responses, leading to sensitivities in particle trajectories.

The BHM-SVW-OEF method seems to be more effective than EEPS-OEF in generating changes in the jets around the

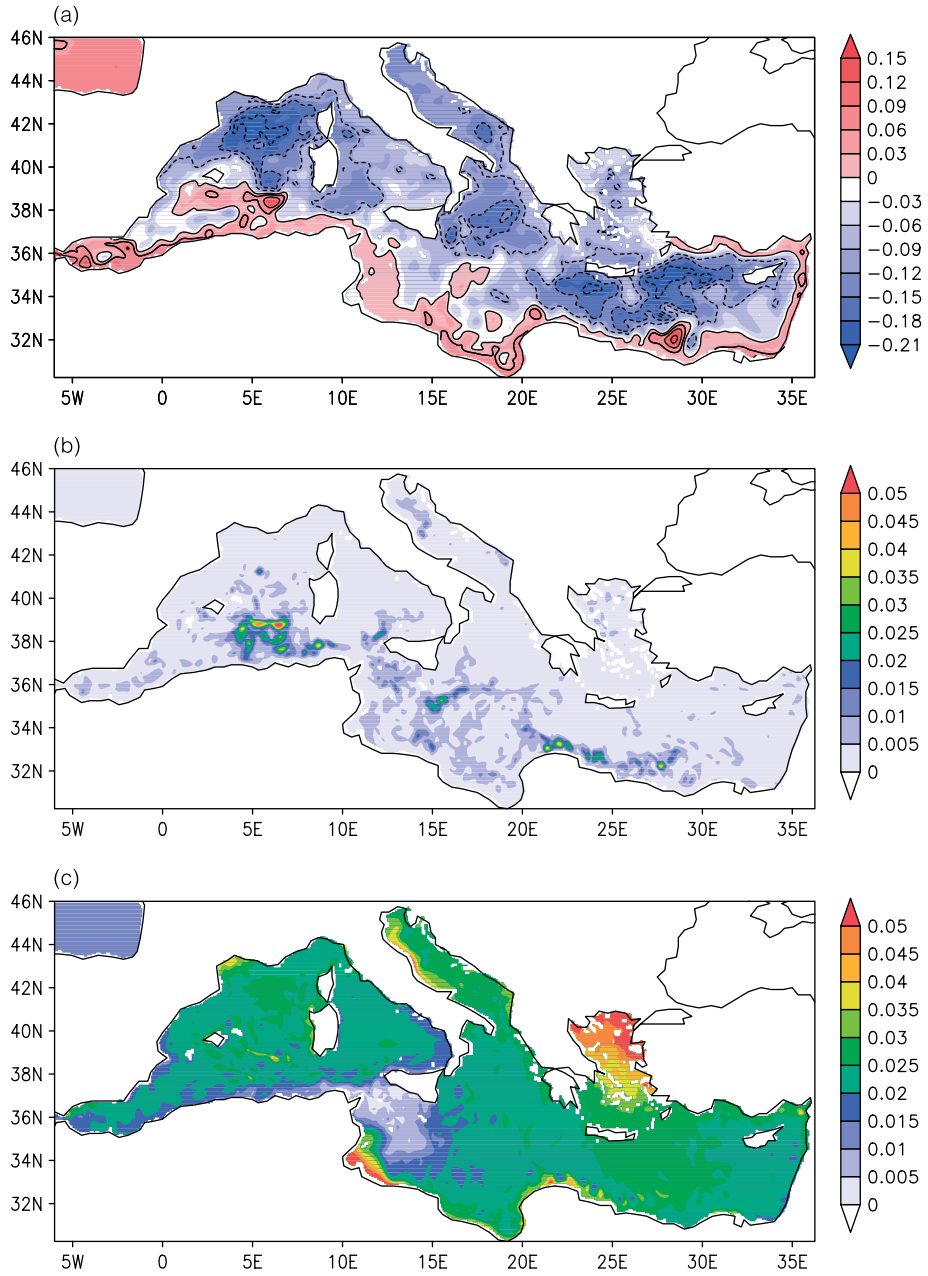

Figure 4. MFS1671 SSH fields for 17 February 2005, last day of forecast period (10*F*). (a) Control forecast daily mean SSH (contour interval is 0.03 m). (b) Standard deviation (m) of SSH from BHM-SVW-OEF at 10*F*. (c) Standard deviation (m) of SSH from EEPS-OEF at 10*F*. The contour interval in (b) and (c) is 0.05 m.

anticyclone and the interaction of the anticyclone with nearby mesoscale eddies. The pinch-off of the border of an anticyclone, the merging of two eddies and the cyclogenesis near an anticyclone are all familiar processes associated with nonlinear barotropic/baroclinic instabilities of open-ocean eddies (McWilliams *et al.*, 1983; Pinardi and Robinson, 1987). The BHM-SVW-OEF method seems to be capable of amplifying, in one week, the initial-condition perturbations on the time- and space-scales of the open-ocean baroclinic/barotropic instability processes.

The mixed instability process manifests itself in the convoluted behaviour of the eddy borders and merging of different size eddies (Pinardi and Robinson, 1986; Masina and Pinardi, 1993). These adjustment processes are manifested in the SSH structures shown in Figure 5. Furthermore, in Figure 6 we provide further support to the interpretation of baroclinic instability, showing a density section across the Algerian current anticyclonic eddy at 5°E, 39°N. High values of BHM-SVW-OEF density spread are found down to 400 m (Figure 6(b)), consistent with a process of mixed instability of open-ocean eddy borders (Pinardi and Robinson, 1987). EEPS-OEF does not perturb the pycnocline of the anticyclonic eddy, only the surface density of the cyclonic eddy north of it (see Figure 5), and it alters the pycnocline structure of the Algerian current. The wind perturbations from both BHM-SVW and EEPS can produce subsurface ocean responses that can persist for many months after the event, thus showing the temporally delayed effects of surface forcing uncertainties. The ocean response associated with perturbed wind forcing is a nonlinear function of the ocean dynamics present in the region of forcing.

We argue that the different ocean ensemble spread vertical structure is directly related to the different scales of the SVW

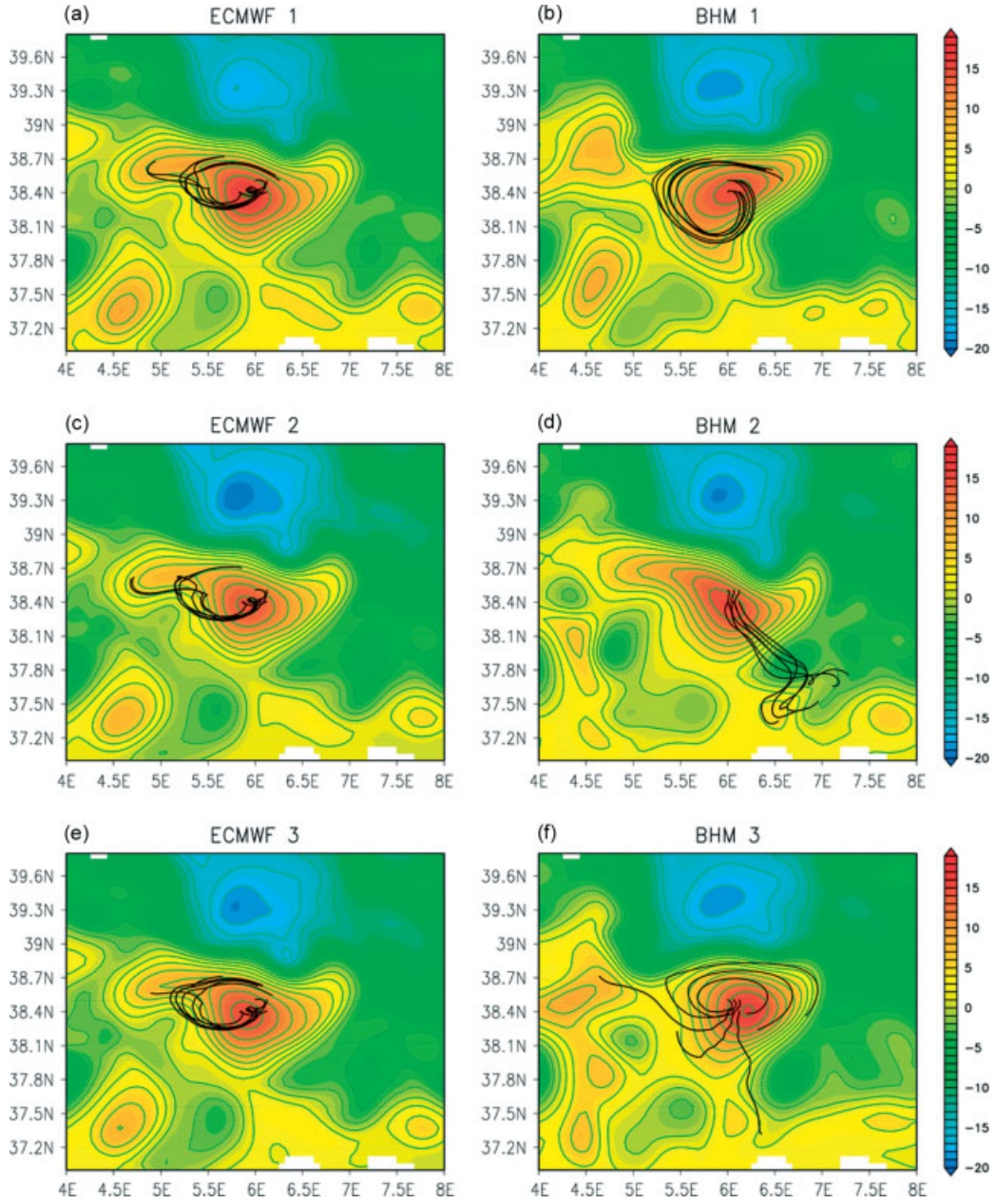

Figure 5. MFS1671 SSH mean daily fields at day 10*F* (17 February 2005) and six simulated particle trajectories (black lines) for EEPS-OEF members 1–3 (panels (a), (c), (e)) and for BHM-SVW-OEF members 1–3 (panels (b), (d), (f)). The contour interval is 0.01 m. Trajectories depict simulated drifter paths from 1*F*–10*F*.

fields. In the BHM-SVW-OEF case, the spread is amplified around the unstable eddy jets, enabling multiple realizations of a process of barotropic/baroclinic instability, while in the EEPS-OEF case the spread is at lower amplitude and suggestive of large-scale, surface-intensified modes.

4.2. *Low-resolution model ensemble response*

In this section we study the response of the lower resolution forecasting model, MFS471, to the BHM-SVW-OEF and EEPS-OEF wind ensemble spread for the canonical ensemble experiment. We expect that the BHM-SVW-OEF method will be sensitive to the model resolution, since the method amplifies the unstable modes associated with ocean mesoscales and the MFS471 model is not eddy-resolving (the Rossby radius of deformation is 10–15 km in the Mediterranean Sea). The MFS471 is started from the upscaled initial condition at 1*A*, so the impact of low resolution is present throughout the analysis and forecast periods.

Figure 7 shows the effects of the lower resolution model in the control forecast SSH (top panel), which is smoother than the equivalent field of Figure 4. In the BHM-SVW-OEF spread (middle panel) the maxima are somewhat localized as in the high-resolution case, but the amplitudes are lower (below 1 cm everywhere). The BHM-SVW-OEF method does not seem to be as effective at low resolution in amplifying the wind perturbations in the ocean response in the horizontal or vertical (not shown). On the other hand, the EEPS-OEF low-resolution experiment exhibits a similar response to the corresponding high-resolution case in terms of both structures and amplitude. The localized spread areas (i.e. Algerian Current, Mersa Matruh gyre, etc.) are missing in the EEPS-OEF low-resolution case and

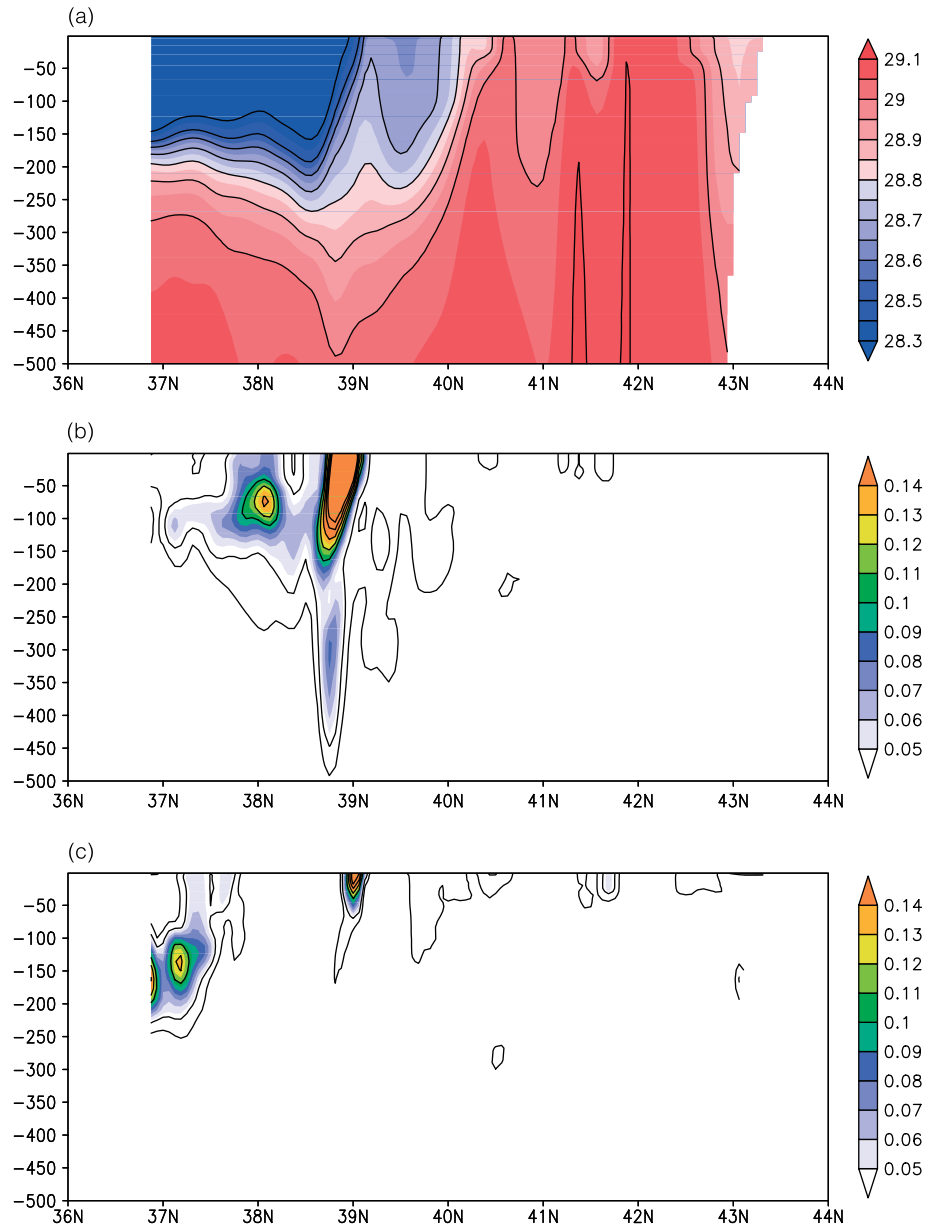

Figure 6. Meridional section of $\sigma = \rho - 1000$ (kg m^{-3}) at 5°E (Algerian coast to the left, French coast to the right) for 17 February 2005 (10*F*). (a) MFS1671 daily mean σ for the control forecast at 10*F*. The contour interval is 0.1 kg m^{-3}. b) σ standard deviation for BHM-SVW-OEF at 10*F*. (c) σ standard deviation of EEPS-OEF at 10*F*. The contour interval in panels (b) and (c) is 0.01 kg m^{-3}.

the large-scale uniform response is dominant. The overall response is less sensitive to the model resolution than in the BHM-SVW-OEF case. This result supports the notion that the new method, BHM-SVW-OEF, amplifies the uncertainty due to winds on ocean mesoscales, while EEPS-OEF mainly changes the uniform, large-scale SSH patterns.

5. Comparison with an initial-condition perturbation method

In this section we compare the wind ensemble perturbation methods above with a more traditional initial-condition perturbation method. Pinardi *et al.* (2008) have developed a thermocline intensified random perturbation ocean ensemble forecast method (TIRP-OEF) that prescribes initial perturbations with an ad hoc horizontal and vertical structure.

The temperature and salinity perturbed initial conditions, T_p and S_p, are written as

$$T_\mathrm{p}(x,y,z,t_0) = T(x,y,z,t_0) + p(x,y)\sum_{j=1}^{M} e_j f_j(z), \qquad (2)$$

$$S_\mathrm{p}(x,y,z,t_0) = S(x,y,z,t_0) + p(x,y)\sum_{j=1}^{M} e_j g_j(z), \qquad (3)$$

where t_0 is the initial time, T and S are the temperature and salinity fields at 14*A*, $p(x,y)$ is a two-dimensional horizontal structure field with random amplitude and $f_j(z)$ and $g_j(z)$ are pre-defined vertical structure functions with amplitudes e_j. This method was originally used to generate Kalman-filter background-error ensembles in Evensen (2003) and extended by Pinardi *et al.* (2008) with vertical structure functions.

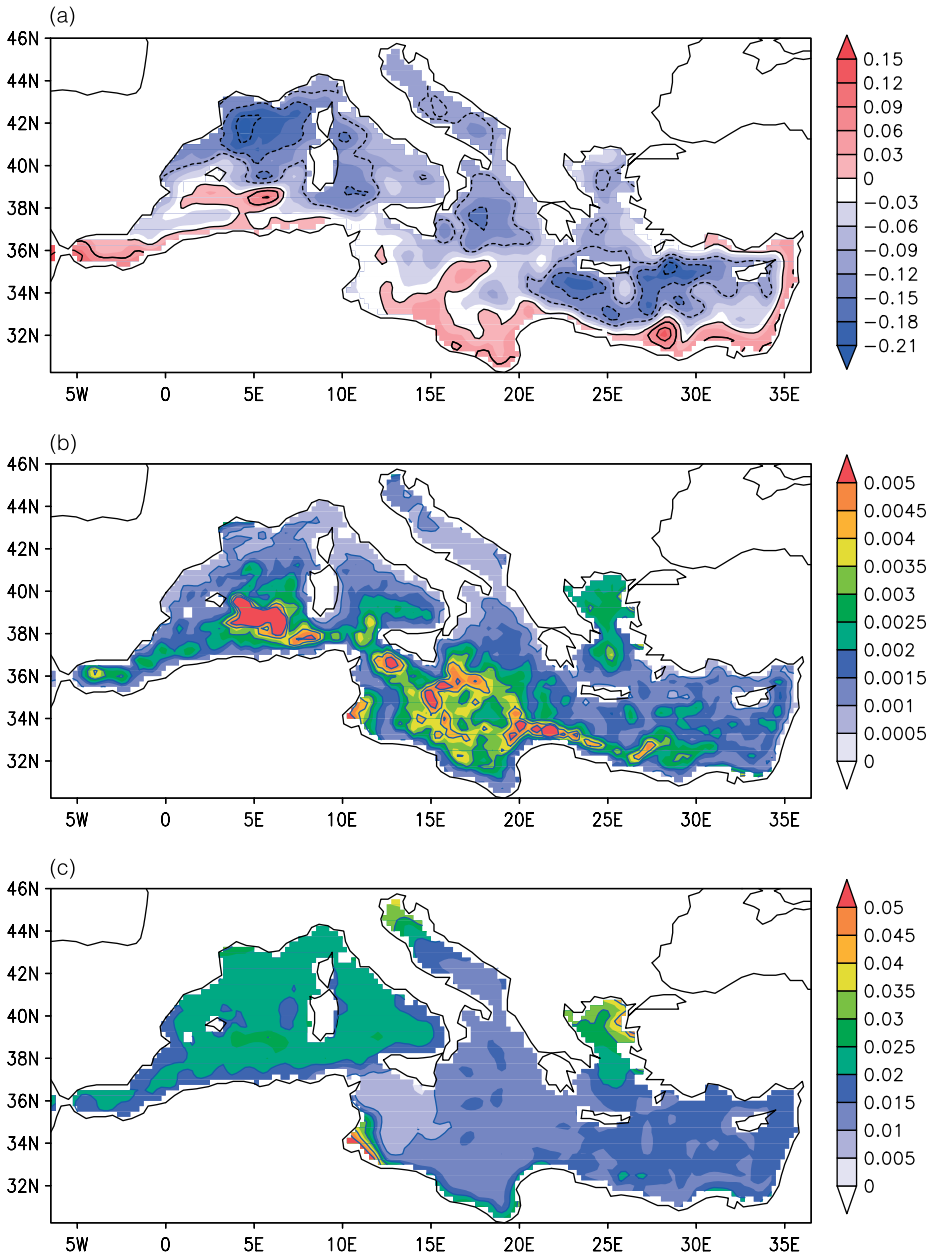

Figure 7. MFS471 SSH fields for 17 February 2005, last forecast day (10*F*). (a) Daily mean SSH fields from the control forecast, contour interval is 0.05 m. (b) Standard deviation (m) of SSH for BHM-SVW-OEF. (c) Standard deviation (m) of SSH for EEPS-OEF . The contour interval in panel (b) is 0.0005 m and that in panel (c) is 0.005 m.

For this experiment, 20 vertical structure functions were selected from a set of EOFs computed from the analysis of the variance of a long ocean model simulation. The e_j are the explained variances or eigenvalues for each mode. The EOFs have maximum amplitude at the depth of the thermocline, around 100–200 m, and they are discussed in Pinardi *et al.* (2008), Dobricic *et al.* (2005) and Sparnocchia *et al.* (2003). The p field at each grid point is modelled by a Gaussian function with a decay radius of 60 km that roughly mimics the size of large mesoscale eddies in the Mediterranean Sea. The amplitude of p was set in order to obtain horizontally integrated perturbations up to a value of ± 0.2 cm in the SSH initial states. Initial perturbations of greater amplitude generate a noise signal in the forecast ensemble spread that does not allow clear identification of dynamical patterns in the forecast response (not shown).

The TIRP perturbations are clearly not consistent with data assimilation, since each point in the domain has the same probability to be perturbed, regardless of whether or not an observation has been assimilated close by. Furthermore it is a method not strictly related to the wind-driven response and is ad hoc in that all free parameters (i.e. the number and type of EOFs, the horizontal structure radius and the amplitude) are decided on the basis of experience.

The TIRP-OEF method implemented here produces 10 perturbed initial T and S fields for the MFS1671 model. The initial-condition ensemble members are forced by the single deterministic ECMWF wind forecast from 8–17 February 2005.

In Figure 8 we show the TIRP-OEF spread at 10*F*. The values are relatively large, up to 4 cm, and they are preferentially organized around mesoscale circulation structures. Three maxima of SSH spread can be identified

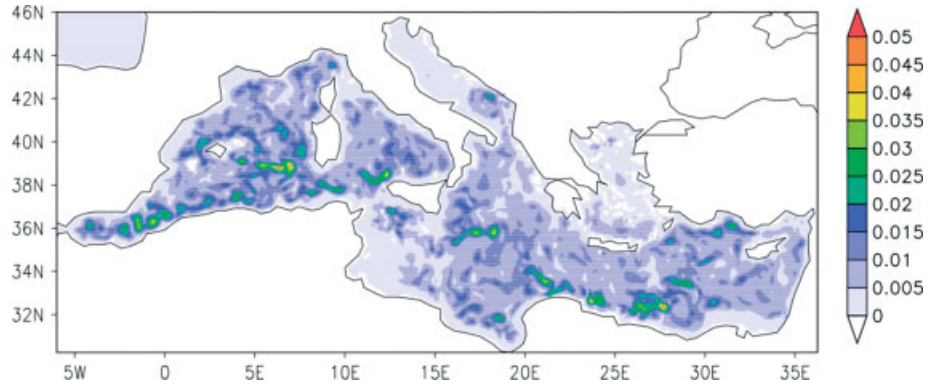

Figure 8. TIRP-OEF SSH standard deviation (m) at 10*F*. The contour interval is 0.005 m.

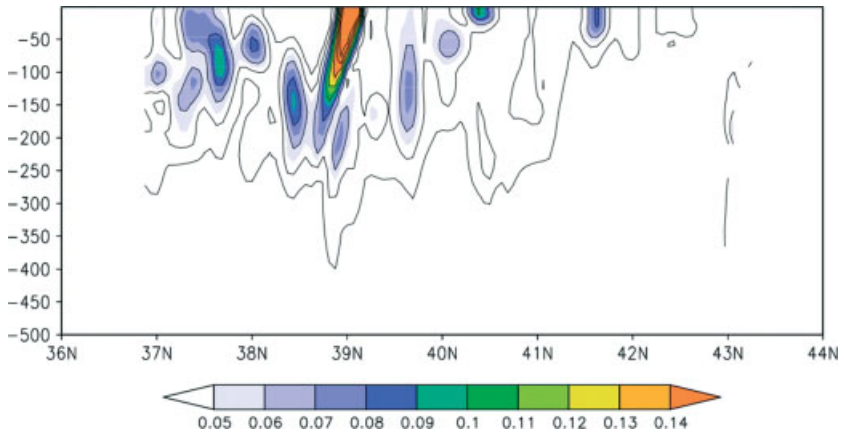

Figure 9. $\sigma = \rho - 1000$ (kg m^{-3}) field standard deviation of TIRP-OEF at 10*F*. The contour interval is 0.01 kg m^{-3} .

in the Algerian current, Ionian Sea and Levantine basin around the Mersa Matruh gyre, as in the case of BHM-SVW-OEF. The section at 5°E (Figure 9) reveals a density-spread structure similar to that observed in the BHM-SVW-OEF experiment (Figure 6(b)), but at slightly smaller amplitude and shallower depths. The BHM-SVW-OEF and TIRP-OEF methods seem to have commensurate forecast ocean responses; more so than for BHM-SVW-OEF and EEPS-OEF. This suggests that the two ensemble methods activate similar dynamical processes.

We argued above that the BHM-SVW spread is associated with ocean mixed barotropic–baroclinic instability processes. The TIRP perturbations are designed to produce modifications of the initial vertical stratification, thus changing the potential energy of the initial field at the thermocline, and potentially activating baroclinic/barotropic instabilities. Comparing Figures 4, 6, 8 and 9, it is evident that both methods can produce spread growing around either localized circulation structures, such as the Mersa-Matruh gyre and the Ionian Stream, or mesoscale open ocean eddy fields, such as the anticyclonic eddy of the Algerian current. The TIRP-OEF spread, however, depends on the choices of the initial vertical EOFs (not shown) and the initial random amplitude. It will be difficult to generalize TIRP-OEF even in the Mediterranean Sea, where the thermocline depth changes are seasonal and the field is dominated by mesoscale eddies.

6. Ensemble variance versus forecast and model errors

A set of 47 BHM-SVW-OEF experiments of the same kind as described in the previous sections was performed for the period January–December 2006. Ensemble forecasts are produced once a week and there is no propagation of ensemble uncertainties between successive OEF cycles. Each cycle is considered to be independent even if the OEF initial conditions at day 1*A* are only one week apart and they are all coming from the sequential analysis cycle of MFS. The nearly one-year-long experiment allows us to check the properties of the BHM-SVW-OEF spread for a period of time that covers an entire cycle of formation and destruction of the thermocline. It also allows us to compare this spread response with the forecast and model error variance.

In a perfect model scenario, wherein it is assumed that the model numerical integration does not introduce any error, the variance associated with the ensemble members around their ensemble mean is an optimal estimate of the forecast error. If M is the number of OEF cycles, and each cycle is composed of N members, then Leutbecher and Palmer (2008) demonstrate that under the perfect model assumption the following limit is satisfied:

$$\lim_{M\to\infty} \frac{1}{M}\sum_{m=1}^{M} \gamma = 0 \qquad \text{and} \qquad \gamma = 1 - \frac{(N+1)\sigma_m^2}{(N-1)\epsilon_m^2}, \tag{4}$$

where $\sigma_m^2 = \langle (X^m - \overline{X}^m)^2 \rangle$ is the variance of the mth OEF cycle, X is in our case the temperature or salinity field at different depths and ϵ_m^2 is the mean-square error of the mth ensemble, computed as the difference between the ensemble mean and the truth, considered here to be the XBT and Argo observations. In our specific case we also compute the average of ϵ_m^2 and σ_m^2 between 1*F* and 10*F*.

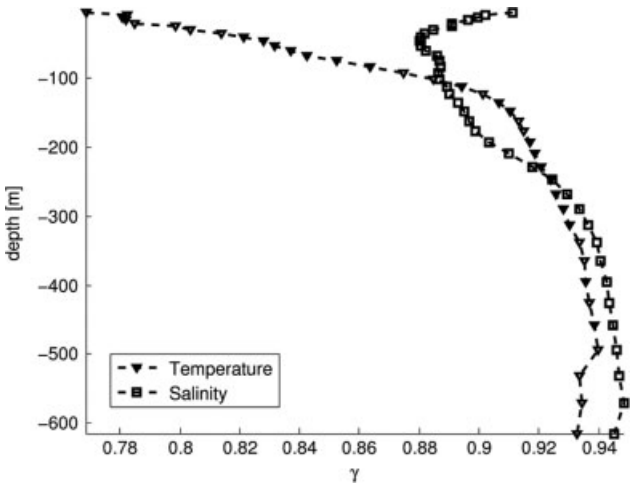

Figure 10. Values of γ (see text) as a function of depth and for temperature and salinity fields for the period January–December 2006 and averaging between day 1*F* and 10*F* values.

In real applications the limit of γ usually differs from zero. Negative values of γ indicate overdispersive ensemble behaviour, i.e. the ensemble forecast variance is larger than the mean-squared forecast error. Positive values of γ indicate underdispersive ensembles, i.e. the ensemble variance is too small compared with the mean-squared error. For instance, Powell *et al.* (2009) show that the Intra American Seas ocean ensemble prediction system had values of $\gamma = -0.32$ and $\gamma = 0.88$ for SSH and SST respectively. The overdispersive behaviour of SSH in Powell *et al.* (2009) was artificially induced by inertia-gravity waves generated by the unbalanced initial conditions. Underdispersive ensembles are usually more common than overdispersive ensembles (Houtekamer and Mitchell, 2001).

The BHM-SVW-OEF is always underdispersive, as shown in Figure 10. Over a series of 47 ensemble prediction cycles we found values of $\gamma = 0.89$ for SSH (not shown), while values for temperature and salinity range between 0.7 and 0.95. Underdispersive minimum values are found in Figure 10 between 0 and 100 m for temperature and between 30 and 200 m for salinity. This result quantifies what was found before for the January–February 2005 study case. The BHM-SVW-OEF method amplifies the ensemble spread in the surface layer (0–100 m) and in the main thermocline (100–200 m), but is not efficient in exciting all forms of uncertainties that contribute to the total forecast error. In fact, the BHM-SVW-OEF method maps only the forecast uncertainties that project on to the possible errors in the wind fields over the 14 day analysis cycle, and it is reasonable that it will underestimate the total forecast error.

Another estimate of the forecast system error is given by the rms of the difference between the model simulation during analysis time and the observations, i.e. the so-called misfit (Dobricic *et al.*, 2007). The rms of the misfit quantifies the errors due to data scarcity, data-assimilation inadequacies and the limited representation of processes by the numerical model. The rms of the misfit is typically used as the estimate of the background field or first-guess errors. We compare the vertical BHM-SVW-OEF ensemble spread with the rms of the misfit to show how much of the background error field the BHM-SVW-OEF method captures in different seasons.

Figure 11 shows that summer intensification of the rms misfit is reproduced by the BHM-SVW-OEF method but the amplitude is largely underestimated (i.e. note the changing grey-scales in Figure 11). This large underestimation is partially due to data scarcity in the computation of the misfits when compared with the ensemble spread computed over every grid point in the discretized Mediterranean domain. The BHM-SVW-OEF method is capable of producing, without any ad hoc assumptions, seasonal errors due to the formation of the thermocline, which is the most significant error source in ocean forecasting models, associated with the forcing inaccuracies and the mesoscale eddy field. The slowly evolving error fields in the subsurface, shown by Figure 11, could also be carried forward so as to amplify the signal in subsequent assimilation forecast cycles. These results indicate that the BHM-SVW-OEF method could be used in the future to produce ensemble members that can quantify the model background-error covariance matrix.

So far we have been looking at the properties of the ensemble variance, trying to understand the ocean response to perturbations from different surface forcings, but the question of how effective the ensembles are in reducing forecast error has yet to be discussed. Available buoy and satellite data support limited forecast verifications for the three ensemble methods compared in this article. For the period January–December 2006 there were 22 ARGO profiles, 77 XBT temperature profiles and 55 satellite tracks of SSH providing 1761 estimates of SLA. These data were compared with the 10 day forecasts for the year. Table I shows the forecast errors versus these data for (a) a single forecast forced by deterministic forecast ECWMF winds and (b) the ensemble mean forecasts for the three ensemble methods compared in this article. The BHM-SVW OEF skill scores match those of the control. The EEPS-OEF temperature rms is slightly smaller than the control, but the SLA rms is larger. The TIRP-OEF skills are worse than control for all comparisons. At this early stage of development, the BHM-SVW OEF ensemble mean forecasts are not better on average than a single deterministic forecast. In fact, the verification statistics of Table I are averaged over the entire Mediterranean and this does not highlight the uncertainty localization properties of the BHM-SVW-OEF method.

7. Conclusions

In this article we have studied different methods of ocean ensemble forecasting applied to the Mediterranean Sea. We have developed a new method, called BHM-SVW-OEF, that uses the posterior realizations of winds coming from the BHM-SVW distributions described in Part I of our work (Milliff *et al.*, 2011). The method produces initial-condition perturbations during a 14 day analysis cycle leading up to the 10 day forecast period by forcing with the BHM-SVW realizations. Part I of this article shows that initial-condition spread in SSH and SST is localized in high-shear and eddy-rich regions during the analysis cycle. Continuing with the BHM-SVW realizations in the forecast period, perturbations grow, doubling in amplitude in ten days. The BHM-SVW-OEF method generates an ocean forecast spread that is concentrated in the ocean mesoscale eddy field. The variance on this scale is probably connected to mixed barotropic/baroclinic instabilities of the open ocean flow field.

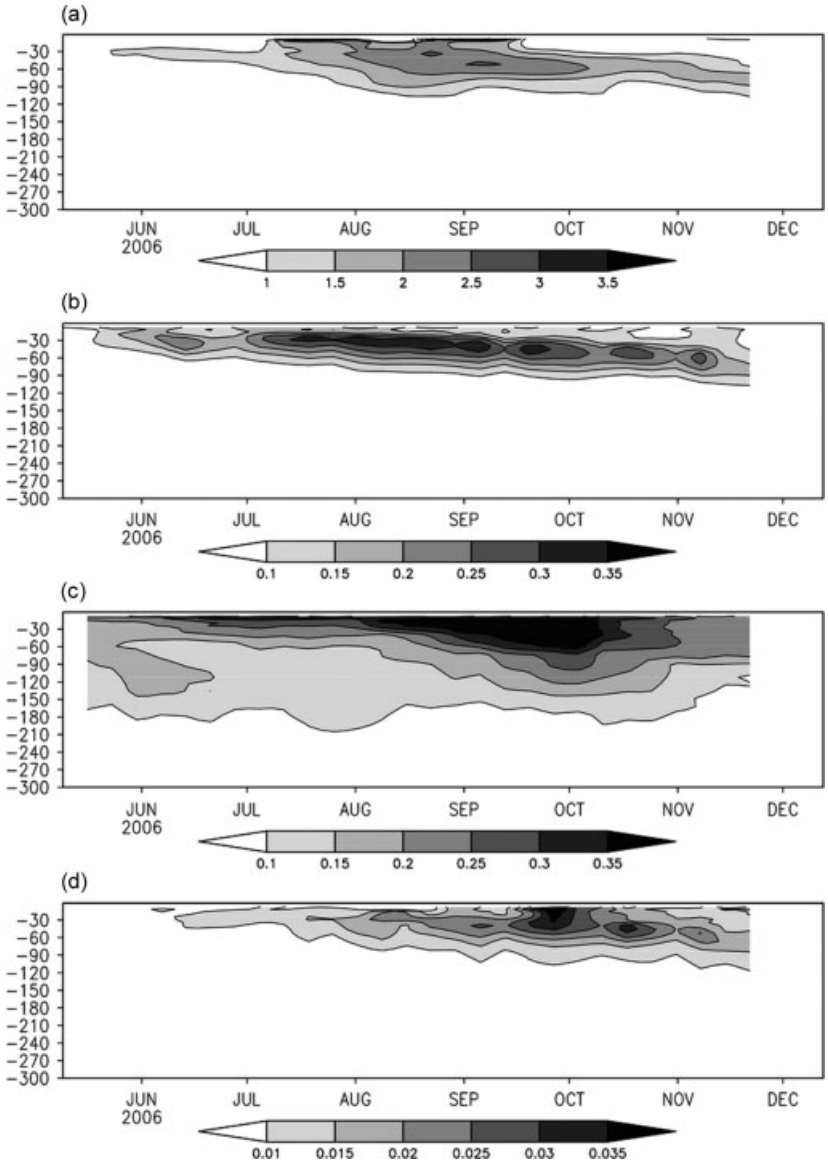

Figure 11. Vertical distribution of temperature and salinity rms of misfits and BHM-SVW-OEF ensemble spread averaged for the whole Mediterranean Sea for the period June–December 2006. (a) Rms of misfit and (b) BHM-SVW-OEF spread for temperature in °C. (c) Rms of misfit and (d) BHM-SVW-OEF spread for salinity in PSU.

Table I. Root-mean-square (rms) errors of forecasts for the period January–December 2006 for temperature, salinity and sea-level anomaly (SLA). Units are°C, psu and m. The rms is calculated as an average over the entire Mediterranean Sea for all vertical levels ('All'), at 30 and 100 m.

Forecast	Temperature			Salinity			SLA
	All	30 m	100 m	All	30 m	100 m	
Deterministic forecast	0.37	0.41	0.4	0.18	0.28	0.22	0.04
BHM-SVW-OEF	0.36	0.41	0.34	0.18	0.28	0.23	0.04
EEPS-OEF	0.36	0.39	0.39	0.18	0.28	0.22	0.05
TIRP-OEF	0.43	0.50	0.48	0.20	0.30	0.25	0.05

The new method has been compared with two more traditional methods of generating ocean ensemble perturbations and forecasts. The first uses the EEPS surface winds starting from a single initial condition and forcing the ocean forecast ensemble with 10 realizations. The second is an ad hoc perturbation method for the T and S initial condition fields, i.e. the so-called thermocline intensified random perturbation (TIRP).

BHM and EEPS winds differ substantially during the forecast time. EEPS wind ensemble spread mimics the forecast error growth in the ten-day forecast period while BHM-SVW ensemble spread is constant over the same

period. This is probably a shortcoming of the BHM-SVW assumptions that can readily be improved in future versions. In contrast, during the analysis period, the BHM-SVW distributions carefully track sources of surface wind forcing uncertainty. This uncertainty can be quantified in an objective way (Chin *et al.*, 1998; Milliff *et al.* 1999, 2004) using abundant scatterometer and analysis data so as to yield realistic estimates of the wind uncertainties. EEPS winds instead try to maximize uncertainty in the growth of errors for the atmospheric forecast focused on middle-troposphere geopotential-height dynamics. The EEPS-SVW realizations exhibit large-scale differences in the surface winds (associated with synoptic disturbances with a scale of several hundred km), while the BHM-SVW realizations differ at finer scales (see Figure 3). Our results show that the finer scale differences in the BHM-SVW realizations can amplify the perturbations on ocean eddy scales much more efficiently than the EEPS-SVW realizations.

Furthermore, the EEPS-SVW fields are not able to alter the vertical stratification of the water column sufficiently, while the BHM-SVW-OEF vertical density spread peaks at the pycnocline of the eddies and retains significant amplitudes below. The BHM-SVW-OEF method activates a vertical, thermocline density ensemble spread that is much larger and more eddy-intensified than the one generated by the EEPS-OEF method. EEPS winds have been successfully applied to probabilistic modelling of ocean waves (Roulston *et al.*, 2005), where depth-intensified response is less important. Our results suggest that short-term ocean circulation forecasts show a limited response to EEPS SVW realizations, mainly confined to the surface and at basin scales.

The experiments conducted with high- and low-resolution ocean models and the BHM and EEPS SVW realizations show a very different forecast response for the two methods. While the EEPS-OEF method yields almost identical ensemble spread between high- and low-resolution experiments, the BHM-SVW-OEF spread amplitude and structure depend crucially on the high-resolution model eddy-field representation. As such, the BHM-SVW-OEF method will be particularly useful for coastal ocean forecasting systems, where the uncertainty due to winds is very important and high resolution is mandatory.

The comparison between BHM-SVW-OEF and TIRP-OEF methods demonstrates analogous responses in the ensemble spread generated by the two methods. The TIRP-OEF and the BHM-SVW-OEF produce thermocline intensified responses on ocean mesoscales, with the former slightly more effective in the horizontal and equivalent to the latter for the vertical ensemble spread. However, the TIRP method is not connected to data-assimilation constraints and is sensitive to the EOF modes chosen. The TIRP-OEF method is ad hoc and needs to be customized, probably on seasonal and interannual time-scales, for general applications.

Ensemble techniques are generally evaluated in terms of their ability to reduce and account for forecast error. We have shown that the BHM-SVW-OEF method does not fully represent the forecast or background field errors. In fact only a small percentage of the forecast error is accounted for in terms of ocean BHM-SVW-OEF spread. However, the vertical structure of the ensemble density spread mimics the background field errors well, being peaked at the thermocline and seasonally varying in depth (Figure 11).

At this research stage of development, we argue that the BHM-SVW-OEF offers a competitive method of producing short-term ocean ensemble forecasts if compared with other, more conventional, methods. Furthermore, it starts from an objective evaluation of uncertainty in the atmospheric forcing for the ocean models and it avoids discontinuities in variance between analysis and forecast periods. The BHM-SVW-OEF method is the only one that can provide consistent wind realizations during both analysis and forecast cycles for an oceanographic ensemble forecasting system. This ensures continuity between the analysis and forecast periods, avoiding the excitement of large-scale gravity-wave mode disturbances due to artificial changes in the surface winds. A natural extension of this work will be the consideration in the BHM-SVW of time-varying wind-variance errors for the forecast period and the combination of ad hoc TIRP perturbations with BHM-SVW during the analysis period.

Acknowledgements

The primary source of support for this work is the Physical Oceanography Program (Code 322) of the US Office of Naval Research (ONR), Dr Manuel Fiadeiro, Program Manager. Additional funding has been provided by ONR-Global to support scientific visits for Nadia Pinardi, and by the University of Bologna, Doctorate Program in Geophysics, and the Istituto Nazionale di Geofisica e Vulcanologia for Alessandro Bonazzi. The computing resources were kindly offered by the Istituto Nazionale di Geofisica e Vulcanologia, Sezione di Bologna, Gruppo Nazionale di Oceanografia Operativa. As with many interdisciplinary collaborations, the time required to complete the companion articles presented here was longer than expected. This delay prevented Professor Pinardi and Dr Milliff from making a deadline (in another journal) for articles honouring the memory of their mentor, Professor Allan R. Robinson. Pinardi and Milliff are currently working on an extension of the work presented here that will be dedicated to Professor Robinson.

References

Andreu-Burillo I, Caniaux G, Gavart M, De Mey P, Baraille R. 2002. Assessing ocean-model sensitivity to wind forcing uncertainties. *Geophys. Res. Lett.* **29**(18): 5.1–5.4.

Auclair F, Marsaleix P, De Mey P. 2003. Space-time structure and dynamics of the forecast error in a coastal circulation model of the Gulf of Lions. *Dyn. Atmos. Oceans* **36**: 309–346.

Brankart JM, Pinardi N. 2001. Abrupt cooling of the Mediterranean Levantine intermediate water at the beginning of the eighties: observational evidence and model simulation. *J. Phys. Oceanogr.* **31**: 2307–2320.

Buizza R. 2006. 'The ECMWF ensemble prediction system'. In *Predictability of Weather Climate*, Palmer T, Hagedorn R (eds). Cambridge University Press: Cambridge, UK.

Buizza R, Palmer TN. 1995. The singular-vector structure of the atmospheric general circulation. *J. Atmos. Sci.* **52**: 1434–1456.

Buongiorno-Nardelli B, Larnicol G, D'Acunzo G, Santoleri R, Marullo S, LeTraon P-Y. 2003. Near real time SLA and SST products during 2 years of MFS pilot project: processing, analysis of the variability and of the coupled patterns. *Ann. Geophys.* **21**: 103–121.

Chin TM, Milliff RF, Large WG. 1998. Basin-scale, high wave number sea surface wind fields from a multiresolution analysis of scatterometer data. *J. Atmos. Oceanic Technol.* **15**: 741–763.

Dobricic S, Pinardi N, Adani M, Bonazzi A, Fratianni C, Tonani M. 2005. Mediterranean Forecasting System: a new assimilation scheme for Sea Level Anomaly and its validation. *Q. J. R. Meteorol. Soc.* **131**: 3627–3642.

Dobricic S, Pinardi N, Adani M, Tonani M, Fratianni C, Bonazzi A, Fernandez V. 2007. Daily oceanographic analyses by Mediterranean Forecasting System at basin scale. *Ocean Sci.* **3**: 149–157.

Evensen G. 2003. The Ensemble Kalman Filter: theoretical formulation and practical implementation. *Ocean Dyn.* **53**: 343–367.
Farrell BF. 1990. Small error dynamics and the predictability of atmospheric flow. *J. Atmos. Sci.* **47**: 2191–2199.
Houtekamer PL, Mitchell HL. 2001. A sequential ensemble Kalman filter for atmospheric data assimilation. *Mon. Weather Rev.* **129**: 123–137.
Isern-Fontanet J, García-Ladona E, Font J. 2006.. The vortices of the Mediterranean sea: an altimetric perspective. *J. Phys. Ocean.* **36**: 87–103.
Kersalé M, Doglioli AM, Petrenko AA. 2010. Sensitivity study of wind forcing in a numerical model of mesoscale eddies in the lee of Hawaii islands. *Ocean Sci. Discuss.* **7**: 477–500.
Korres G, Pinardi N, Lascaratos A. 2000. The ocean response to low frequency interannual atmospheric variability in the Mediterranean Sea, Part I: Sensitivity experiments and energy analysis. *J. Climate* **13**: 705–731.
Lacarra J, Talagrand O. 1988. Short-range evolution of small perturbations in a barotropic model. *Tellus* **40A**: 81–95.
Le Traon PY, Nadal F, Ducet N. 2003. An improved mapping method of multisatellite altimeter data. *J. Atmos. Oceanic Technol.* **15**: 522–533.
Leutbecher M, Palmer TN. 2008. Ensemble forecasting. *J. Comput. Phys.* **227**: 515–539.
Lucas M, Ayoub N, Penduff T, Barnier B, De Mey P. 2008. Stochastic study of the temperature response of the upper ocean to uncertainties in the atmospheric forcing in an Atlantic OGCM. *Ocean Modelling* **20**: 90–113. DOI:10.1016/j.ocemod.2007.07.006.
Manzella GMR, Reseghetti F, Coppini G, Borghini M, Cruzado A, Galli C, Gertman I, Gervais T, Hayes D, Millot C, Murashkovsky A, Ozsoy E, Tziavos C, Velasquez Z, Zodiatis G. 2007. The improvements of the ships of opportunity program in MFS-TEP. *Ocean Sci.* **3**: 245–258.
Masina S, Pinardi N. 1993. The halting effect of baroclinicity in vortex merging. *J. Phys. Oceanogr.* **23**: 1618–1637.
McWilliams JC, Brown ED, Bryden HL, Ebbesmeyer CC, Elliot BA, Heinmiller RH, Hua BL, Leaman KD, Lindstrom EJ, Luyten JR, McDowell SE, Owens WB, Perkins H, Price JF, Regier L, Riser SC, Rossby HT, Sanford TB, Shen CY, Taft BA, Van Leer JC. 1983. 'The local dynamics of eddies in the western North Atlantic'. In *Eddies in Marine Science*, Robinson AR (ed). Springer-Verlag: Berlin, pp 92–113.
Milliff RF, Large WG, Morzel J, Danabasoglu G, Chin TM. 1999. Ocean general circulation model sensitivity to forcing from scatterometer winds. *J. Geophys. Res.* **104**: 11337–11358.
Milliff RF, Freilich MH, Liu WT, Atlas R, Large WG. 2001. 'Global ocean surface wind vector observations from space'. In *Observing the oceans in the 21st Century*, Koblinsky CJ, Smith NR (eds). GODAE Project Office and Bureau of Meteorology: Melbourne.
Milliff RF, Morzel J, Chelton DB, Freilich MH. 2004. Wind stress curl and wind stress divergence biases from rain effects on QSCAT surface wind retrievals. *J. Atmos. Oceanic Technol.* **21**: 1216–1231.
Milliff RF, Bonazzi A, Wikle CK, Pinardi N, Berliner LM. 2011. Ocean ensemble forecasting. Part I: Ensemble Mediterranean winds from a Bayesian hierarchical model. *Q. J. R. Meteorol. Soc.* DOI: 10.1002/qj.767.
Pettenuzzo D, Large WG, Pinardi N. 2010. On the corrections of ERA-40 surface flux products consistent with the Mediterranean heat and water budgets and the connection between basin surface total heat flux and NAO. *J. Geophys. Res.* **115**: C06022. DOI:10.1029/2009JC005631.
Pinardi N, Coppini G. 2010. Operational oceanography in the Mediterranean Sea: the second stage of development. *Ocean Sci.* **6**: 263–267.
Pinardi N, Robinson AR. 1986. Quasigeostrophic energetics of open ocean regions. *Dyn. Atmos. Oceans* **10**: 185–221.
Pinardi N, Robinson AR. 1987. Dynamics of deep thermocline jets in the polymode region. *J. Phys. Oceanogr.* **17**: 1163–1188.
Pinardi N, Allen I, Demirov E, DeMey P, Korres G, Lascaratos A, LeTraon P-Y, Maillard C, Manzella G, Tziavos C. 2003. The Mediterranean Ocean Forecasting System: first phase of implementation (1998–2001). *Ann. Geophys.* **21**: 49–62.
Pinardi N, Bonazzi A, Scoccimarro E, Dobricic S, Navarra A, Ghiselli A, Veronesi P. 2008. Very large ensemble ocean forecasting experiment using the grid computing infrastructure. *Bull. Am. Meteorol. Soc.* **89**: 799–804.
Poulain PM, Barbanti R, Font J, Cruzado A, Millot C, Gertman I, Griffa A, Molcard A, Rupolo V, Bras SL, de-la Villeon LP. 2007. Medargo: a drifting profiler program in the Mediterranean Sea. *Ocean Sci.* **3**: 379–395.
Powell BS, Moore AM, Arango HG, DiLorenzo E, Milliff RF, Leben RR. 2009. Near real time assimilation and prediction in the Intra-American Sea with Regional Ocean Modelling System. *Dyn. Atmos. Oceans* **48**: 46–68.
Roulston MS, Ellepola J, von Hardenberg J, Smith LA. 2005.. Forecasting wave height probabilities with numerical weather prediction models. *Ocean Eng.* **32**: 1841–1863.
Sparnocchia S, Pinardi N, Demirov E. 2003. Multivariate empirical orthogonal function analysis of the upper thermocline structure of the Mediterranean Sea from observations and model simulations. *Ann. Geophys.* **21**: 167–187.
Tonani M, Pinardi N, Dobricic S, Pujol I, Fratianni C. 2008. A high-resolution free-surface model for the Mediterranean Sea. *Ocean Sci.* **4**: 1–14.
Tonani M, Pinardi N, Fratianni C, Pistoia J, Dobricic S. 2009. Forecast and analysis assessment through skill scores in the Mediterranean Sea. *Ocean Sci.* **5**: 649–660.

